Clinical Neurology and Neurosurgery 204 (2021) 106596

Contents lists available at ScienceDirect

Clinical Neurology and Neurosurgery

journal homepage: www.elsevier.com/locate/clineuro

Influence of Virchow-Robin spaces on the electric field distribution in subthalamic nucleus deep brain stimulation

Fabiola Alonso [a,*], Peter Zsigmond [b], Karin Wårdell [a,c]

[a] Department of Biomedical Engineering, Linköping University, Sweden
[b] Department of Neurosurgery and Department of Biomedical and Clinical Sciences, Linköping University, Sweden
[c] Center for Medical Image Science and Visualization, Linköping University, Linköping, Sweden

ARTICLE INFO

Keywords:
Deep brain stimulation (DBS)
Subthalamic nucleus (STN)
Virchow-Robin spaces
Parkinson's disease
Patient-specific model
Directional leads

ABSTRACT

Patient MRI from DBS implantations in the subthalamic nucleus (STN) were reviewed and it was found that around 10% had Virchow-Robin spaces (VRS). Patient-specific models were developed to evaluate changes in the electric field (EF) around DBS leads. The patients (n = 7) were implanted bilaterally either with the standard voltage-controlled lead 3389 or with the directional current-controlled lead 6180. The EF distribution was evaluated by comparing simulations using patient-specific models with homogeneous models without VRS. The EF, depicted with an isocontour of 0.2 V/mm, showed a deformation in the presence of the VRS around the DBS lead. For patient-specific models, the radial extension of the EF isocontours was enlarged regardless of the operating mode or the DBS lead used. The location of the VRS in relation to the active contact and the stimulation amplitude, determined the changes in the shape and extension of the EF. It is concluded that it is important to take the patients' brain anatomy into account as the high conductivity in VRS will alter the electric field if close to the DBS lead. This can be a cause of unexpected side effects.

1. Introduction

Virchow-Robin spaces (VRS) are small cavities or cysts which were initially reported as autopsy findings in the globus pallidus and putamen by Dechambre already in 1838 [1]. Previous investigations by Laitinen et al., in 1990 using 1 Tesla MRI have shown the appearance of VRS in the basal ganglia and their relationship with parkinsonian symptoms [2]. With the advent of more advanced MR scanners and protocols, VRS have also been identified as small areas with similar intensity signal to that of the cerebrospinal fluid (CSF) in T1 or T2-weighted images [3]. The presence of VRS within the subthalamic nucleus (STN) is however scarcely reported [4–6].

Assuming a correct selection of the patient, the success of DBS surgery is highly dependent on placing the stimulating electrode at the optimal location, and the fine tuning of the stimulation parameters. While the location of the electrode can be confirmed with a post-operative computer tomography scan (CT), the effect of the stimulation parameters can only be estimated and visualized with the aid of computer models or indirectly through the patient response.

Computer models based on the finite element method (FEM) can calculate the bioelectric fields generated during the stimulation and estimate the amount of neural activation around the electrodes. Different methodologies have been used to estimate and visualize the stimulation field, either including neuronal models [7,8] or inferring the neural activation based on specific electric field isolevel [9–12]. The present study uses the latter method to evaluate the influence of changes in the surrounding medium on the electric field distribution. The interest relies particularly in the presence of VRS found in the subthalamic nucleus of parkinsonian patients.

The effect of VRS using FEM models was studied by our group more than ten years ago [13], where the VRS were modelled as spheres with high electrical conductivity, corresponding to that of the CSF surrounded by homogeneous grey matter. Simulations showed that the electric field around the deep brain stimulation electrodes is affected due to the presence of VRS.

The aim of this study was to investigate the influence of these highly conductive regions in the STN using patient-specific 3D models. The electric field was visualized with a fixed isolevel to enable comparisons

Abbreviations: CSF, Cerebrospinal fluid; CT, Computer tomography; DBS, Deep brain stimulation; EF, Electric field; FEM, Finite element method; H, Homogeneous; IPG, Implantable pulse generator; MRI, Magnetic resonance imaging; PD, Parkinson's disease; PS, Patient-specific; STN, Subthalamic nucleus; VRS, Virchow-Robin spaces.

* Corresponding author. Present/Permanent address: Department of Biomedical Engineering, Campus US, Linköping University, SE-581 83 Linköping, Sweden.

https://doi.org/10.1016/j.clineuro.2021.106596
Received 15 May 2020; Received in revised form 12 October 2020; Accepted 2 March 2021
Available online 9 March 2021

of the electric field between models with and without VRS.

2. Materials and methods

2.1. Patient data

Pre-operative MR images from 69 patients with Parkinson's disease operated between 2007 and 2017 at the Department of Neurosurgery, Linköping University Hospital were examined to identify the presence of VRS in the STN. From this set, images from seven patients (six male and one female, aged between 59 and 70, mean 64.5 years) implanted in the STN that presented VRS were selected and used to create patient-specific FEM models. Informed written consent was received from the patients and the study was approved by the local ethics committee in Linköping (2012/434-31). A 3 Tesla Phillips Ingenia (Phillips Medical Systems, Eindhoven, The Netherlands) T2-weighted MRI with 2 mm contiguous axial slices ($2 \times 0.5 \times 0.5$) mm^3 were taken preoperatively from six patients while one of the patients was imaged with a 1.5 T Phillips Achieva dStream scanner. The location of the leads was confirmed postoperatively through a computer tomography (CT) the day after surgery co-registered with the preoperative MRI. From this merged batch, the surgeon noted the Leksell coordinates from artefacts of the most distal electrode and from another one higher up, at the anterior commissure-posterior commissure plane. These were used for the placement of the leads in the brain model.

2.2. FEM model

The finite element model consists of the DBS leads surrounded by the conductive medium, i.e. the brain tissue. The leads were modelled according to the geometry specified by the manufacturing company [11] (Fig. 1) and located according to the coordinates noted by the surgeon. The patient-specific brain tissue was modelled with an in-house MatLab developed software ELMA [10,14], using the preoperative T2-weighted images from each one of the seven patients.

In ELMA [15], the preoperative MRI batch is first reduced to several slices at the level of interest (typically 40 slices, 2 mm thick) and then cropped to a region of interest (ROI) around the target, resulting in a specific cuboid model for each patient brain. Within that ROI, relevant tissue types are segmented according to the image intensity values and assigned with the corresponding electrical conductivity: grey ($\sigma = 0.123$ S/m), white matter ($\sigma = 0.0754$ S/m), cerebrospinal fluid ($\sigma = 2$ S/m) and blood ($\sigma = 0.7$ S/m). The VRS were classified as CSF due to their brightness. The electrical conductivity was assigned from tabulated data [16] and weighted with the spectral content of the pulse shape [17]. An interpolation function was used to assign the conductivity values to each voxel to consider the effect of partial volumes. Thus, voxels with intensity levels between e.g. grey and white matter, receive an electrical conductivity in between. The resulting interpolation matrix with the conductivity values was subsequently used as the material property matrix in the FEM models, having the same resolution as the preoperative MRI data set. For more details regarding the use of ELMA please see [10,14].

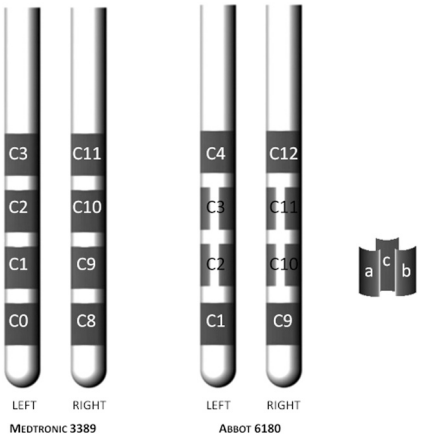

Fig. 1. Schematic description of the lead models. Contacts named according to the manufacturing company indicating the implantation site. The eight channel lead 6180 segmented contacts are sub indexed, e.g. $C10_{a,b,c}$.

The 3D finite element models were built using the commercial software Comsol Multiphysics v5.4 (Comsol AB, Stockholm, Sweden). The Leksell coordinates provided by the surgeon were transformed to Cartesian coordinates and used to place the leads within the brain model.

The electric field was calculated by the equation for steady currents:

$$\nabla \cdot \boldsymbol{J} = -\nabla \cdot (\sigma \nabla V) = 0 \quad (\mathrm{A/m3}) \tag{1}$$

where $\boldsymbol{J}$ is the current density (A/m^2), V the electrical potential (V) and σ is the electrical conductivity (S/m) that corresponds to the interpolation matrix extracted by ELMA. The boundary conditions correspond to a cathodic monopolar configuration, except for patient 6 and 7 (Table 1). Thus, for patients 1–5, the active contacts were set to either voltage or current controlled source and the outer boundaries of the cuboid were set to ground ($V = 0$). The inactive contacts were set to floating potential ($\int -\boldsymbol{n} \cdot \sigma \nabla V dS = 0$ (A); $\boldsymbol{n} \times (-\nabla V) = 0$ (V/m)) and the non-conductive surfaces were set to electric insulation ($\boldsymbol{n} \cdot \nabla V = 0$ (V/m)) where $\boldsymbol{n}$ is the surface normal vector.

The mesh applied was determined by the physics having a denser mesh where higher gradients occur, i.e. close to the active contacts. The models were solved with the iterative Comsol built-in conjugate gradients solver. The models consisted in ~3 million degrees of freedom.

Three of the seven patients were implanted with the directional lead 8 CH Infinity model 6180 (Abbot Inc. Saint Paul, MN, USA). The lead was set in ring mode by activating all contacts from the same level (Table 1). The rest of the patients were implanted with the conventional lead 3389 (Medtronic Inc. Minneapolis, MN, USA), Fig. 1.

2.3. Simulations

2.3.1. Clinically set parameters

Simulations (n = 14) were run using the stimulation parameters clinically set 4–6 weeks after implantation (Table 1). The electric field obtained with the homogeneous (H) and patient-specific (PS) models was investigated.

2.3.2. Steering function

A hypothetical scenario was designed to evaluate the potential benefit of directional leads to steer the stimulation field. For this purpose, the model for patient 1 and the lead at the right side were used.

Table 1
Parameters clinically set and used for the patient-specific stimulations.

Patient	Lead	Stimulation amplitude		Pulse width (μs)	Ground
		Left	Right		
1	6180	$C2_{a,b,c}$: 0.5 mA	$C10_{a,b,c}$: 3.3 mA	90	IPG Case
2	3389	C1: 2.0 V	C9: 2.0 V	60	IPG Case
3	6180	$C2_{a,b,c}$: 3.3 mA	$C10_{a,b,c}$: 3.3 mA	60	IPG Case
4	6180	$C2_{a,b,c}$: 3.55 mA	$C10_{a,b,c}$:2.8 mA	60	IPG Case
5	3389	C2:3.1 V	C9: 3.1 V	60	IPG Case
6	3389	C2&C3: 2.3 V	C9&C10:0.7 V	60	IPG Case
7	3389	C1: 3.7 V	C8, C9&C10: 1.8 V	120	C2&C3 / IPG Case

C stands for contact followed by its number, and the subscripts a, b, c refer to each face of the split contact of the directional lead 6180.

First, two faces of the split contact C10 (c, b) were activated and then only one (b) of the faces was active. The active contacts were chosen to be at the opposite side of the VRS. The stimulation amplitude was set from 0.5 to 4.5 mA in steps of 0.2 mA. The same procedure was applied for the homogeneous model to investigate the effect of the VRS.

2.4. Data analysis

The number of VRS were counted in both hemispheres of all patients. The electric field magnitude was visualized with a 0.2 V/mm isolevel and superimposed on the corresponding preoperative MRI for both, the patient-specific and the homogeneous models. The EF isocontours were displayed on the orthogonal anatomical planes placed at the target coordinates (Fig. 2). The extension of this isolevel and the volume within the isosurface were compared between the patient-specific and the homogeneous grey matter models. The EF extension (mm) was measured from the center of active contact i.e. from the target coordinates (x_t, y_t, z_t) to the furthest point of the isocontour (0.2 V/mm). The measurements were performed over the corresponding anatomical planes: axial, sagittal and coronal (Fig. 2).

The EF volume (mm^3) within the isosurface was calculated with a built-in integration function in Comsol.

Relative differences were calculated for the electric field extension and volume between the patient-specific (EF_{PS}) and the homogeneous (EF_H) models, considering the EF obtained from the homogeneous model as the reference:

$$Relative\ dif. = \frac{EF_{PS} - EF_H}{EF_H} \quad (2)$$

For the cases where VRS were present at the target level, the distance from the border of the VRS to the surface of the electrode was measured in Comsol Multiphysics.

3. Results

All patients presented VRS in the STN. A total of 24 with 16% more VRS (14) at the left hemisphere than the right hemisphere (10). The number of VRS per patient were 2 in average (1–4) at the left side and 1.4 (1–2) at the right.

3.1. Clinically set parameters

Simulations showed that the electric field distribution is affected by the VRS. The higher electrical conductivity of these regions in the vicinity of the electrode redistributes the electric field pushing it away from the VRS. The same effect occurs regardless of the operating mode or the lead design if the directional lead is configured in ring mode. A summary of the EF volumes within the 0.2 V/mm isosurface is presented in Table 2 and the corresponding graph in Fig. 3.

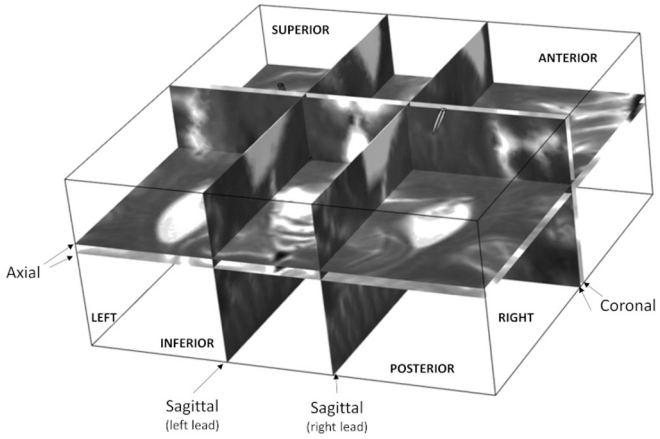

Fig. 2. Cut planes used to visualize the electric field isocontour and measure its extension. Planes crossing at the target coordinates for each lead.

VRS at the level of the targets were present in 6 of the 7 patients. Table 3 presents the location of the VRS and the maximum extension of the EF for homogeneous and patient-specific models. Distances were measured between the surface of the active contact and the border of the VRS. All the measurements were performed at the axial plane at the target level except for patient 6, who presented the VRS below the target thus the distance to the VRS was measured at the sagittal plane. For patient 6, the maximum extension registered was also at the sagittal plane (SFig. 4D).

For patient 1, VRS were present in both hemispheres but only those at the right side affected the electric field. The VRS at the right side is visible from the target level to 2 mm below it, as shown in Fig. 4A. The effect of the VRS was clearly visible at the axial and sagittal view. The VRS at the left side is outside the EF isocontour showing no effect on its shape or extension.

3.2. Steering function

The activation of two electrodes at the opposite direction to the VRS was capable to steer the field and avoid the VRS up to a certain stimulation amplitude. For higher stimulation amplitudes the field started to surround the electrode losing directionality. Fig. 5 shows the EF isocontours at the axial plane for both models at different stimulation amplitudes. The electric field generated by only one face of the split electrode is presented in the video (Fig. 6), displayed at the axial view at the target level. The EF isocontour for the homogeneous model corresponds to 3.1 mA while for the patient-specific model the EF is shown for an increasing stimulation amplitude.

4. Discussion

Finite element models based on patient-specific images have been developed to evaluate the effect of Virchow-Robin spaces in the electric field distribution around DBS electrodes. The simulations showed a deformation of the electric field depending on the VRS location in relation to the active contacts and the stimulation amplitude. VRS that are in contact with the active electrode modify the spatial distribution of the electric field by extending it in the direction of the VRS. The higher electrical conductivity of the VRS avoids a drop of potential in those regions redistributing the electric field around them. This was also shown in the modelling approach by Åström et al. [13]. For the cases where the VRS are not within the radial extension of the electric field or the stimulation amplitude is not high enough for the EF to reach the VRS, then there is no visible effect on the specific isolevel used. This was observed using the clinically set stimulation parameters for the left lead of patient 1 and the right lead of patient 6 (Fig. 4 and SFig 4, respectively).

The comparison of the EF volumes within the isosurfaces between the homogeneous and patient-specific simulations did not indicate the presence of VRS by its own. The EF volume obtained from the patient-specific models was larger than that from the homogeneous. This responds to the difference in the electrical conductivity of the electrode's surrounding indicating a lower electrical conductivity for the patient-specific models compared with the homogeneous grey matter. The effect of the VRS, nevertheless, was clear for patient 1 where the "holes" created by the VRS resulted in a smaller EF volume.

The EF volume can also be influenced by the encapsulation layer surrounding the electrode. Previous studies [11,18] have included an encapsulation layer around the entire lead to mimic the electrode-brain interface at different time points after the lead is implanted. It was shown that the EF for chronic conditions (assumed to have low electrical conductivity) is attenuated. For acute conditions (high electrical conductivity) a shunting effect occurs. The models for this study did not

Table 2
Electric field volume within the 0.2 V/mm isosurface for each clinical case, for homogeneous (EF_H) and patient-specific (EF_{PS}) simulations.

Patient	Lead	Stimulation amplitude		Left volume (mm^3)		Right volume (mm^3)		Difference (%)	
		Left	Right	EF_H	EF_{PS}	EF_H	EF_{PS}	Left	Right
1	6180	0.5 mA	3.3 mA	7.0	10.0	138.0	129.0	37.7	– 6.5
2	3389	2 V	2 V	90.0	94.5	90.0	84.1	4.7	– 7.0
3	6180	3.3 mA	3.3 mA	137.6	230.8	137.7	200.9	71.9	38.7
4	6180	3.55 mA	2.8 mA	146.5	208.1	105.7	126.1	43.7	28.3
5	3389	3.1 V	3.1 V	151.2	194.6	151.5	180.1	28.4	17.5
6	3389	2.3 V	0.7 V	203.4	214.1	24.5	28.1	5.3	14.7
7	3389[1]	3.7 V	1.8 V	175.2	283.2	162.0	181.5	61.6	12.0

[1] Bipolar stimulation with contacts C1 & C2 grounded (Table 1).

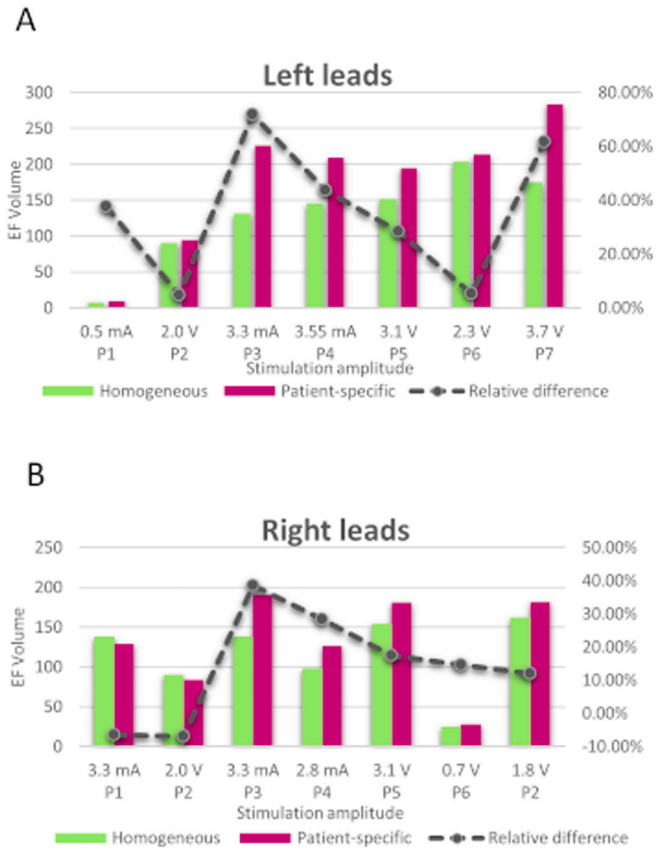

Fig. 3. Relative difference between the volumes within the EF_{PS} and EF_H isosurfaces for all patients at the left (A) and right (B) hemisphere.

Table 3
Location of Virchow Robin spaces and maximum extension of the electric field at the target level, for homogeneous (EF_H) and patient-specific (EF_{PS}) simulations.

Patient	Stimulation amplitude	Side	VRS distance (mm)	Maximum extension (mm)	
				EF_H	EF_{PS}
1	3.3 mA	Right	0.2	3.3	5.6
2	2 V	Left	3.6	2.7	3.1
3	–	No VRS	–	–	–
4	3.55 mA	Left	0.7	3	4.3
5	3.1 V	Right	2.5	3.3	3.8
6	2.3 V	Left	0.4	3.7	5.7
7	1.8 V	Right	0–3 mm	3	6.5

consider this interface due to the uncertainty of the effect of the VRS touching the electrode. This might overestimate the extension of the EF but made it possible to isolate the effect of the VRS on the EF distribution.

The extension of the electric field isocontour was larger at all planes for all patients. The shape of the EF was enlarged towards the VRS, surrounding it in some cases (patients 1, 6 and 7). This effect may result in the stimulation of regions that are far from the target reducing the therapeutic window and increasing the possibility of the presence of side effects, especially if the deformation occurs laterally, e.g. towards the internal capsule [19]. The present study does not include postoperative symptoms assessment because none of the patients presented side effects. The VRS for the patients studied were located either anterior, posterior or medially in relation to the lead, thus even large deformations of the electric field such as in patient 1 (Fig. 4) did not result in side effects for the patient.

The extension of the EF isocontour roughly corresponds to the stimulation amplitude applied, i.e. the EF isocontour extends ~3 mm for 3 mA (slightly larger for voltage) as shown in Table 3. Similar stimulation radiuses have been reported [20] or estimated [21]. Thus, if the VRS is located within the radius of stimulation, it is very likely that the EF shape and extension will be affected.

The representation of the stimulation field using a fixed EF isolevel for bipolar configuration might not be an optimal estimator since the actual stimulation of neurons passing close to the anodic pole is not considered [22]; the effect of the VRS however, was clearly captured with the simulations for patient 7. In fact, the effect of VRS may be disregarded with other visualization approaches such as potential isosurfaces [23].

4.1. Steering function

The steering function of the directional lead was evaluated through hypothetic scenarios where either one or two electrodes from the split ring were activated. Clinical studies [24,25] have shown that directional leads, when compared with conventional leads, are capable to increase the therapeutic window. Our results showed that turning off the electrode that is close to the VRS may avoid the stimulation of areas beyond that region, potentially reducing the possibility of a side effect. However, according to our results and previous studies [11,26], the steering capability is dependent on the stimulation amplitude used. The electric field isocontours for both, homogeneous and patient-specific models, lost directionality around 2 mA as shown in Fig. 5, SFig 6 and the video (Fig. 6). The presence of VRS in preoperative images becomes important not only to for postoperative programming but also at the planning stage to reconsider the lead trajectory to avoid the VRS or to consider the use of directional leads.

Determining if the side effects are due to the presence of VRS around the electrode is very difficult and in clinical practice is not yet possible to determine with high accuracy the position of the split electrodes. Some studies [27,28] however, have shown the possibility to determine the orientation of the electrodes based on the artefacts shown in

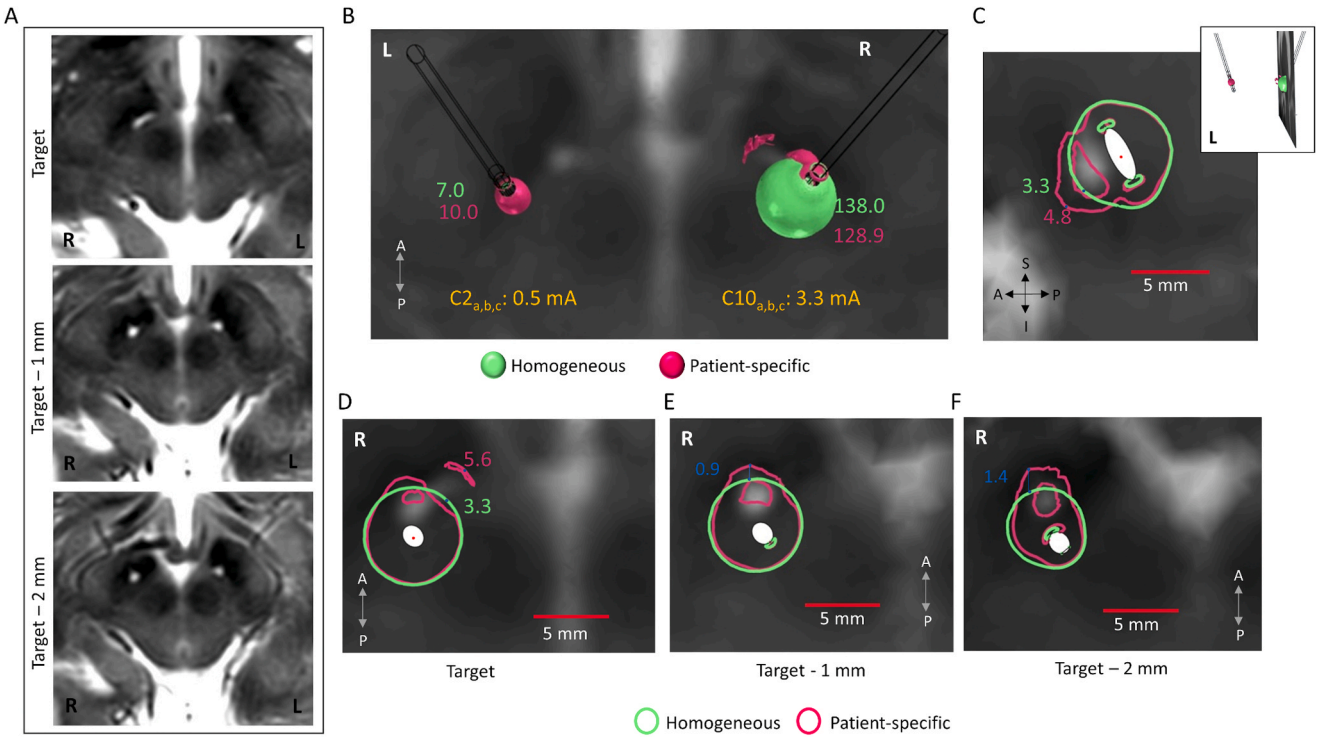

Fig. 4. Patient 1 with lead 6180 in ring mode. **A.** Preoperative MRI axial slices at different levels. **B.** 3D view of the electric field and the corresponding volume (mm^3) within the isosurface obtained for each model (mm^3). **C.** Sagittal view showing the EF deformation. **D–F.** EF isocontours superimposed to the patient MRI at different levels. Distance between the EF_H and EF_{PS} isocontours shown in blue (mm). The VRS at the left side does not affect the EF from that lead.

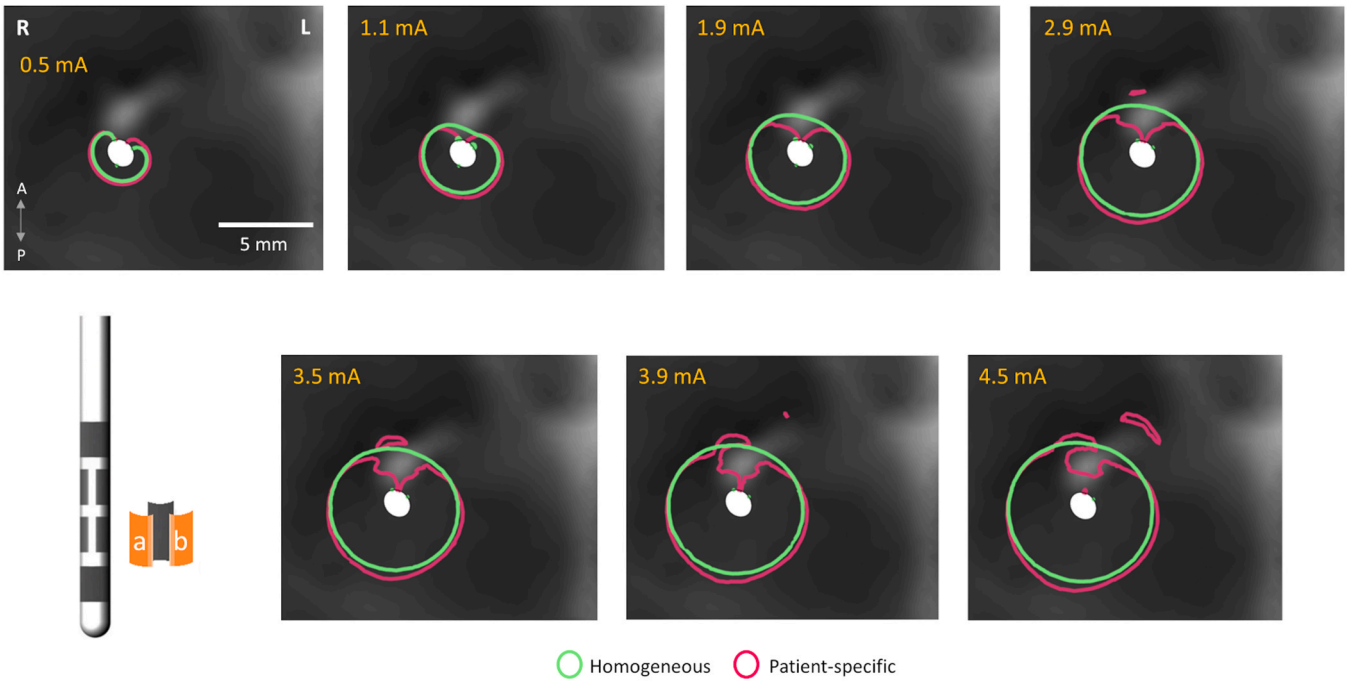

Fig. 5. Patient 1 with lead 6180 in steering mode. Electric field isocontours at the axial plane located at the target level with an increasing stimulation amplitude. Activation of electrodes a and b from the first row of split contacts in Abbot directional lead. The active contacts, shown in orange at the lower panel, are opposite to the VRS. As the stimulation amplitude increases the EF tends to surround the lead.

postoperative CT scans. Regardless the lack of certainty of the position of each electrode, the hypothetic scenarios designed help to understand how the activation of single electrodes may avoid the stimulation at the opposite site of it.

5. Conclusion

The presence of Virchow- Robin spaces in PD patients affects the EF distribution during STN DBS. Their location and the stimulation amplitude determine how the EF is spread. VRS close to the active

contact can result in the stimulation of regions beyond the targeted area. Directional leads can help to avoid VRS using low stimulation amplitudes. The use of patient-specific models has shown the importance of considering nuances of the patients' anatomy, which is not possible with homogeneous models. This information can be used to determine the stimulation parameters and to support the analysis of side effects induced by DBS. In the future, with better understanding of how the segmented contacts are situated it will be easier to predict the effects of the stimulation, and confirm the potential advantage of directional leads assessed by including the patient-specific data in the models.

CRediT authorship contribution statement

Fabiola Alonso: Methodology, Investigation, Writing - original draft, Visualization. **Peter Zsigmond:** Conceptualization, Resources, Investigation, Writing - review & editing. **Karin Wårdell:** Conceptualization, Writing - review & editing, Supervision, Funding acquisition.

Conflicts of interest

We wish to confirm that there are no known conflicts of interest associated with this publication and there has been no significant financial support for this work that could have influenced its outcome.

Acknowledgments

This study was supported by the Swedish Foundation for Strategic Research (SSF BD15-0032) and the Swedish Research Council (VR 2016-03654).

Appendix A. Supporting information

Supplementary data associated with this article can be found in the online version at doi:10.1016/j.clineuro.2021.106596.

References

[1] A. Dechambre, Mémoire sur la curabilité du ramollissement cérébral, Gaz. Med. Paris 6 (1838) 305–314.
[2] L.V. Laitinen, D. Chudy, M. Tengvar, M.I. Hariz, A.T. Bergenheim, Dilated perivascular spaces in the putamen and pallidum in patients with Parkinson's disease scheduled for pallidotomy: a comparison between MRI findings and clinical symptoms and signs, Mov. Disord. 15 (6) (2000) 1139–1144, https://doi.org/10.1002/1531-8257(200011)15:6<1139::aid-mds1012>3.0.co;2-e (Nov).
[3] R.M. Kwee, T.C. Kwee, Virchow-Robin spaces at MR imaging, Radiographics 27 (4) (2007) 1071–1086.
[4] J. Jagid, K. Madhavan, N. Desai, A. Bregy, M. Desai, A. Ruiz, R. Quencer, H. J. Landy, Deep brain stimulation complicated by bilateral large cystic cavitation around the leads in a patient with Parkinson's disease, BMJ Case Rep. 2015 (2015), bcr2015211470, https://doi.org/10.1136/bcr-2015-211470 (Oct 16).
[5] A. Ramirez-Zamora, D. Levine, D.B. Sommer, J. Dalfino, P. Novak, J.G. Pilitsis, Intraparenchymal cyst development after deep brain stimulator placement, Stereotact. Funct. Neurosurg. 91 (5) (2013) 338–341, https://doi.org/10.1159/000350021.
[6] R.W. Murrow, G.D. Schweiger, J.J. Kepes, W.C. Koller, Parkinsonism due to a basal ganglia lacunar state: clinicopathologic correlation, Neurology 40 (6) (1990) 897–900, https://doi.org/10.1212/wnl.40.6.897 (Jun).
[7] C.R. Butson, S.E. Cooper, J.M. Henderson, C.C. McIntyre, Patient-specific analysis of the volume of tissue activated during deep brain stimulation, Neuroimage 34 (2) (2007) 661–670, https://doi.org/10.1016/j.neuroimage.2006.09.034 (Jan 15).
[8] A. Chaturvedi, C.R. Butson, S.F. Lempka, S.E. Cooper, C.C. McIntyre, Patient-specific models of deep brain stimulation: influence of field model complexity on neural activation predictions, Brain Stimul. 3 (2) (2010) 65–67, https://doi.org/10.1016/j.brs.2010.01.003 (Apr).
[9] M. Åström, E. Diczfalusy, H. Martens, K. Wårdell, Relationship between neural activation and electric field distribution during deep brain stimulation, IEEE Trans. Biomed. Eng. 62 (2) (2015) 664–672, https://doi.org/10.1109/TBME.2014.2363494 (Feb).
[10] M. Åström, L.U. Zrinzo, S. Tisch, E. Tripoliti, M.I. Hariz, K. Wårdell, Method for patient-specific finite element modeling and simulation of deep brain stimulation, Med. Biol. Eng. Comput. 47 (1) (2009) 21–28, https://doi.org/10.1007/s11517-008-0411-2 (Jan).
[11] F. Alonso, M.A. Latorre, N. Göransson, P. Zsigmond, K. Wårdell, Investigation into deep brain stimulation lead designs: a patient-specific simulation study, Brain Sci. 6 (3) (2016) 39, https://doi.org/10.3390/brainsci6030039 (Sep 7).
[12] S. Hemm, G. Mennessier, N. Vayssiere, L. Cif, H. El Fertit, P. Coubes, Deep brain stimulation in movement disorders: stereotactic coregistration of two-dimensional electrical field modeling and magnetic resonance imaging, J. Neurosurg. 103 (6) (2005) 949–955, https://doi.org/10.3171/jns.2005.103.6.0949 (Dec).
[13] M. Åström, J.D. Johansson, M.I. Hariz, O. Eriksson, K. Wårdell, The effect of cystic cavities on deep brain stimulation in the basal ganglia: a simulation-based study, J. Neural Eng. 3 (2) (2006) 132–138, https://doi.org/10.1088/1741-2560/3/2/007 (Jun).
[14] J.D. Johansson, F. Alonso, K. Wårdell, Patient-specific simulations of deep brain stimulation electric field with aid of in-house software ELMA. 2019 41st Annual International Conference of the IEEE Engineering in Medicine and Biology Society (EMBC), IEEE, 2019, pp. 5212–5216.
[15] K. Wårdell, J.D. Johansson, M. Åström, E. Dicsfaluzy, ELMA open access app. ⟨https://liu.se/en/article/ne-downloads⟩ (Accessed 2020).
[16] C. Gabriel, A. Peyman, E.H. Grant, Electrical conductivity of tissue at frequencies below 1 MHz, Phys. Med. Biol. 54 (16) (2009) 4863–4878, https://doi.org/10.1088/0031-9155/54/16/002 (Aug 21).
[17] K. Wårdell, L. Zrinzo, M. Hariz, M. Andersson, Patient-specific brain modelling for deep brain stimulation simulations. 2013 6th International IEEE/EMBS Conference on Neural Engineering (NER), IEEE, 2013, pp. 148–151.
[18] N. Yousif, R. Bayford, P.G. Bain, X. Liu, The peri-electrode space is a significant element of the electrode–brain interface in deep brain stimulation: a computational study, Brain Res. Bull. 74 (5) (2007) 361–368.
[19] M. Picillo, A.M. Lozano, N. Kou, R.P. Munhoz, A. Fasano, Programming deep brain stimulation for Parkinson's disease: the Toronto western hospital algorithms, Brain Stimul. 9 (3) (2016) 425–437.
[20] M.S. Nielsen, C. Bjarkam, J. Sørensen, M. Bojsen-Møller, N.A. Sunde, K. Østergaard, Chronic subthalamic high-frequency deep brain stimulation in Parkinson's disease–a histopathological study, Eur. J. Neurol. 14 (2) (2007) 132–138.
[21] A.M. Kuncel, S.E. Cooper, W.M. Grill, A method to estimate the spatial extent of activation in thalamic deep brain stimulation, Clin. Neurophysiol. 119 (9) (2008) 2148–2158.
[22] D.N. Anderson, G. Duffley, J. Vorwerk, A.D. Dorval, C.R. Butson, Anodic stimulation misunderstood: preferential activation of fiber orientations with anodic waveforms in deep brain stimulation, J. Neural Eng. 16 (1) (2019), 016026.
[23] H.C.F. Martens, E. Toader, M. Decré, D.J. Anderson, R. Vetter, D.R. Kipke, K. B. Baker, M.D. Johnson, J.L. Vitek, Spatial steering of deep brain stimulation volumes using a novel lead design, Clin. Neurophysiol. 122 (3) (2011) 558–566.
[24] C. Pollo, A. Kaelin-Lang, M.F. Oertel, L. Stieglitz, E. Taub, P. Fuhr, A.M. Lozano, A. Raabe, M. Schüpbach, Directional deep brain stimulation: an intraoperative double-blind pilot study, Brain 137 (7) (2014) 2015–2026.
[25] F. Steigerwald, L. Müller, S. Johannes, C. Matthies, J. Volkmann, Directional deep brain stimulation of the subthalamic nucleus: a pilot study using a novel neurostimulation device, Mov. Disord. 31 (8) (2016) 1240–1243.
[26] T. Nordin, P. Zsigmond, S. Pujol, C.F. Westin, K. Wardell, White matter tracing combined with electric field simulation - a patient-specific approach for deep brain stimulation, NeuroImage Clin. 24 (2019), 102026, https://doi.org/10.1016/j.nicl.2019.102026.
[27] A. Hellerbach, T. Dembek, M. Hoevels, J. Holz, A. Gierich, K. Luyken, M. Barbe, J. Wirths, V. Visser-Vandewalle, H. Treuer, DiODe: directional orientation detection of segmented deep brain stimulation leads: a sequential algorithm based on CT imaging, Stereo Funct. Neurosurg. 96 (5) (2018) 335–341, https://doi.org/10.1159/000494738.
[28] P.C. Reinacher, M.T. Krüger, V.A. Coenen, M. Shah, R. Roelz, C. Jenkner, K. Egger, Determining the orientation of directional deep brain stimulation electrodes using 3D rotational fluoroscopy, Am. J. Neuroradiol. 38 (6) (2017) 1111–1116.